

Nanomagnetic Control of Intersystem Crossing

Adam E. Cohen[†]

Departments of Chemistry and Chemical Biology and of Physics, Harvard University, 12 Oxford Street, Cambridge, Massachusetts 02138

Received: July 26, 2009

A theory is presented for how magnetic nanostructures can catalyze intersystem crossing in molecular radical pairs. Magnetic field gradients near physically realistic nanostructures are strong enough to induce a relative reorientation of two electronic spins in <1 ns, overwhelming nuclear hyperfine coupling as a driver of intersystem crossing. Nanomagnetic control of intersystem crossing represents a form of heterogeneous catalysis that does not require molecular contact, but only short-range magnetic coupling.

1. Introduction

Can a weak magnetic field affect the outcome of a chemical reaction? At first blush this seems implausible: Zeeman splittings are so much smaller than thermal energy that any effects on equilibrium constants are imperceptibly small. Nonetheless, magnetic field effects (MFEs) have been observed in many nonequilibrium processes that go through a radical pair intermediate.^{1–3} The magnetic field is thought to influence the spin dynamics in the pair and thereby to determine the branching ratio between singlet recombination and triplet dissociation. Here I propose a qualitatively new mechanism by which magnetic nanostructures can significantly enhance the effect of magnetic fields on radical pair processes.

The essence of the argument is that the field due to a magnetic nanostructure may vary significantly over the extent of a single radical pair, causing the two spins to precess at different rates and about different axes. Relative reorientation of two spins leads to intersystem crossing (ISC). Homogeneous magnetic fields, in contrast, are forbidden by symmetry from achieving this relative reorientation, and only affect spin dynamics through higher order processes. Field gradients near physically realistic magnetic nanostructures are strong enough to dominate all other processes that lead to ISC. Nanostructures that may enhance ISC include magnetic nanocrystals, ferromagnetic domain boundaries, and surfaces exhibiting antiferromagnetic or spin density wave order.

Reaction schemes susceptible to MFEs are shown in Figure 1. While a great many variants of these schemes have been observed, the generic features are (1) photoinduced electron transfer to form spin-correlated radical pairs with a singlet:triplet ratio that deviates in either direction from the equilibrium value of 1:3, (2) a period of quantum mechanical spin evolution during which the electrons may interconvert between singlet and triplet states, and (3) a chemical reaction involving either geminate recombination or diffusional separation. Geminate recombination is typically allowed only for the singlet state—a consequence of the Pauli exclusion principle—while diffusional separation is generally open to both the singlet and the triplet states. The branching ratio between recombination and separation depends on the relative rates of recombination, separation, and ISC.

Magnetic field modulated ISC has been detected in the photoconductivity,^{4–6} photoluminescence,⁷ excited-state lifetime,^{8,9}

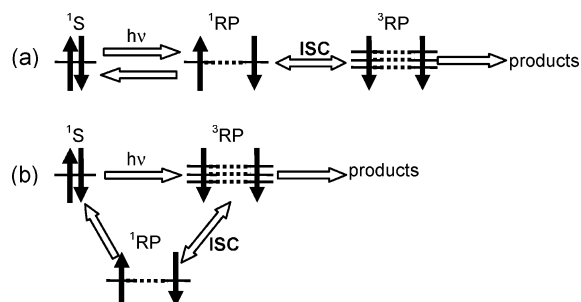


Figure 1. Reaction schemes susceptible to magnetic field effects. (a) Singlet radical pairs are prevented from geminate recombination if ISC converts to a triplet state. (b) Triplet radical pairs can only undergo geminate recombination if ISC converts to a singlet state (the vertical axis is not intended to represent energy). Dotted lines joining the radical pairs indicate that the electrons may reside either on distal parts of one molecule or on two molecules held together in a solvent "cage".

and chemical reactivity¹ of many molecular systems, and even in the dynamics of photosynthesis.¹⁰ Magnetic field effects on the reaction outcome are already known for dozens of photochemical processes.¹¹ Model systems include electron transfer between pyrene and dimethylaniline¹² and in photolysis of benzophenone^{13,14} and dibenzyl ketone.^{15,16} Typically ISC is much slower than diffusional separation in homogeneous solutions, so MFEs are enhanced when reactions are performed in micellar "cages" which keep radical pairs colocalized for an extended time.^{14,17,18} Magnetically active nuclei can become isotopically enriched in photochemical reactions through the influence of the nuclear magnetic field on ISC.^{19,20} Magnetic field modulation of radical pair reactions is speculated to play a role in magnetic navigation in birds^{21–23} and fruit flies²⁴ although this hypothesis remains unproved. Recently, MFEs on spin dynamics in solid-state systems have attracted interest. In particular, semiconductor double dots allow high-resolution studies of ISC at low temperatures,²⁵ and nitrogen-vacancy defects in diamond have been proposed as nanoscopic magnetometers.²⁶

Several recent observations suggest that magnetic nanostructures may induce unusual spin dynamics of electrons in nearby organic molecules. These effects include enhanced quantum efficiency, magnetically modulated quantum efficiency,^{27,28} and magnetoresistance²⁹ in organic LEDs doped with magnetic nanocrystals, and anomalously large magnetic field effects on the outcome of photochemical reactions in solutions doped with

[†] E-mail: cohen@chemistry.harvard.edu

magnetic particles.^{30,31} These phenomena have been interpreted as an enhanced rate of ISC in radical pairs, induced by the magnetic nanostructure. The observed effects, however, are far larger in magnitude *and of the opposite sign* compared to what one would expect from enhancements in the strength of the local magnetic field coupled with the conventional hyperfine mechanism of ISC. However, experiments using magnetic micro-particles in free solution may be confounded by field-induced assembly of the particles into chains or aggregates, which can alter the optical scattering and mass transport properties of the solution. These anomalous experimental results point to the need for a new microscopic model of ISC in magnetically heterogeneous systems, and for clean experiments in which nanomagnetic effects can be distinguished from effects mediated by field-induced particle motion.

In 1933 Wigner proposed that magnetic field gradients from gas-phase paramagnetic species could induce ortho–para nuclear conversion in H₂.³² The magnetic field from a paramagnetic species is different at the locations of the two protons in H₂, inducing a relative reorientation of the protons. Petzinger and Scalapino extended this theory to include encounters between H₂ and magnetically heterogeneous surfaces,³³ and Atkins and Clugston treated diffusive encounters with paramagnetic species in solution.³⁴ The present theory is based on the same physical concept as the Wigner–Petzinger–Atkins (WPA) theory, with the replacement of magnetic nanostructures for paramagnetic ions and electron spins for nuclear spins. Also relevant is the work of Buchachenko on electron spin catalysis, in which ISC is induced by an asymmetric *exchange* interaction between one member of a radical pair and a paramagnetic species in solution.³⁵

While the physical basis of the present discussion is similar to that of WPA, we require a different mathematical approach. WPA treat the interaction using perturbation theory, justified because the probability of a nuclear spin flip during a single encounter is small. In the present case, the interaction is strong enough to induce significant electronic spin evolution, so perturbation theory is not appropriate. Instead, we solve the Schrödinger equation for each magnetic field, and then calculate a two-electron density matrix averaged over all spin trajectories.

Kubo and Toyabe took this latter approach to calculate zero-field relaxation of muon spins in solids.³⁶ Each muon samples a different embodiment of the approximately static, random, nuclear hyperfine fields, and the density matrix is obtained by averaging the spin evolution over all embodiments of the hyperfine field. Measurements of relaxation of spin-polarized muons quantitatively confirm the predictions of the Kubo–Toyabe theory.³⁷

Schulten and Wolynes developed the same argument (apparently independently of Kubo–Toyabe) for hyperfine-induced ISC in radical pairs.^{38,39} Each electron is coupled to approximately static, random, nuclear hyperfine fields. The independent precession of the two electrons leads to ISC. The two-spin relaxation functions of Schulten and Wolynes are closely related to the single-spin relaxation of Kubo and Toyabe (see the Appendix).

We calculate the spin evolution of a radical pair following Kubo and Schulten, but we include fields of a magnetic nanostructure in addition to hyperfine fields. Binhi recently suggested a qualitative model along similar lines, but did not provide a framework for calculations.⁴⁰ The present theory is restricted to radical pairs in which the two electrons are far enough apart that there is negligible contribution to ISC from exchange interactions, dipolar coupling, or spin–orbit coupling.

These other factors are often important in the case of biradicals (i.e., when the two radicals reside on the same molecule).¹⁷ For simplicity we only consider radical pairs starting in a singlet state, although parallel arguments apply to an initial triplet. Simple estimates show that the magnetic inhomogeneity near a nanostructure can exceed that due to hyperfine fields by up to 2 orders of magnitude.

The theory suggests that structures with large magnetic field gradients can catalyze reactions that involve ISC in a radical pair state. External fields that influence the strength or location of the magnetic field gradient will modulate the magnetocatalytic activity. Unlike conventional heterogeneous catalysis, nanomagnetic catalysis is mediated purely by through-space magnetic interactions.

Our results imply that it is not impossible for biogenic magnetic nanoparticles, such as those reported in human brains⁴¹ and other organisms,^{42,43} to play a role in mediating radical chemistry, and for this activity to be more sensitive to weak magnetic fields than was previously thought. Observations of such an effect have been claimed,^{44,45} though conclusive experimental evidence is still lacking.

Section 2 provides a simple semiclassical estimate of the rate of ISC in the presence of a magnetic nanoparticle, and section 3 gives a quantum theory of nanomagnetic enhancement of ISC.

2. Semiclassical Estimate of ISC

ISC occurs when two electron spins undergo a relative reorientation. This reorientation requires that the two spins experience different effective magnetic fields. The local magnetic field may have contributions from (1) hyperfine fields from nearby magnetic nuclei and (2) an externally applied field modulated by the local environment. We restrict ourselves to the case where the electrons are separated by >1 nm, so exchange interactions, spin–orbit coupling, and dipolar interactions can be neglected (the full treatment is given in Kaptein’s papers^{46,47}).

An external magnetic field causes electronic spins to precess on the Bloch sphere at a Larmor frequency $\omega = g\mu_B B/\hbar$, where $\mu_B = 9.3 \times 10^{-24}$ J/T is the Bohr magneton and the Landé *g*-factor of the electron is ~ 2.002 . Equivalently, the electron gyromagnetic ratio is $\gamma = 28$ GHz/T. In an inhomogeneous magnetic field, ISC occurs in approximately the time it takes the two electrons to accumulate a relative phase shift of 180°:

$$\tau_{\text{ISC}}^{-1} \approx \frac{\mu_B}{\pi\hbar}(B\Delta g + g\Delta B) \quad (1)$$

where Δg is the difference in the *g*-factor between the electrons and ΔB is the difference in the local magnetic field (we use the rms difference in the ensemble for ΔB). For well-separated electrons, eq 1 suffices to estimate the rates of magnetic field effects on radical pair reactions.

Hyperfine interactions with nearby magnetically active nuclei cause each electron to experience an approximately random, approximately static effective magnetic field. Typical hyperfine fields are 1–30 G, and thus lead to ISC in 10^{-8} – 10^{-6} s. In the absence of an external field, hyperfine interactions mix all four spin states. An external magnetic field splits the T₊ and T_− states through the Zeeman effect. When this splitting exceeds the hyperfine coupling, these states become energetically inaccessible, so two of the ISC reaction channels are shut off. Thus, a dc magnetic field *decreases* the extent of ISC due to the hyperfine mechanism.

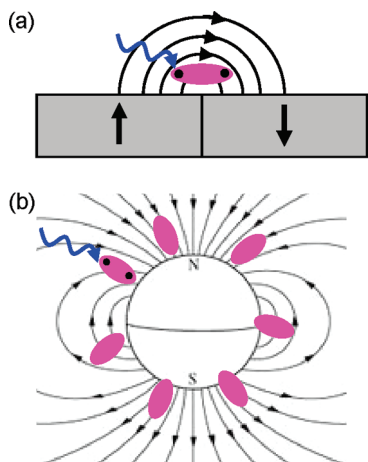


Figure 2. Rates of intersystem crossing are strongly modified by magnetic field gradients near magnetic nanostructures: (a) magnetic domain wall, (b) magnetic nanoparticle.

Local chemical interactions cause each electron to have a slightly different value of g , with typical differences in organic molecules of $\Delta g \approx 10^{-3}$. The “ Δg mechanism” leads to ISC that *increases* with increasing field strength. In an external field of 1000 G, the Δg mechanism leads to ISC in typically 10^{-7} – 10^{-6} s. Neither the HFC nor the Δg mechanism is fast enough to compete with diffusional separation in low-viscosity liquids, which typically occurs in <1 ns, so most magnetic field effects on radical pair processes are small.

2.1. ISC near a Magnetic Nanostructure. In the vicinity of a magnetic nanostructure, magnetic field gradients can be quite strong—strong enough for the field to vary appreciably over the separation between electrons in a radical pair. Each electron experiences a different local magnetic field and precesses at a different rate or about a different axis. Figure 2 illustrates this point for radical pairs near magnetic domain boundaries and near magnetic nanocrystals. We now consider the case of proximity to a nanocrystal in more detail.

How large is ΔB for a radical pair next to a magnetic nanocrystal? We model the nanocrystal as a uniformly magnetized sphere, with magnetic moment \mathbf{m} . The magnetic field outside the sphere is the same as that of a point dipole of moment \mathbf{m} located at the center of the sphere:⁴⁸

$$\mathbf{B}(\mathbf{r}) = \frac{\mu_0}{4\pi r^3} [3(\mathbf{m} \cdot \hat{\mathbf{r}})\hat{\mathbf{r}} - \mathbf{m}] \quad (2)$$

where μ_0 is the permeability of free space. Let \mathbf{l} be the vector connecting the two electrons in a radical pair. Provided that $r \gg l$, we can approximate $\Delta \mathbf{B} \approx \mathbf{l} \cdot \nabla \mathbf{B}$. It is a matter of straightforward but tedious trigonometry to average $\|\mathbf{l} \cdot \nabla \mathbf{B}\|^2$ over all orientations of the vectors \mathbf{r} and \mathbf{l} . Petzinger and Scalapino give a detailed group theoretic discussion of how to evaluate such averages.³³ Taking the average yields

$$\langle |\Delta \mathbf{B}|^2 \rangle^{1/2} \approx \frac{\mu_0}{4\pi} \frac{lm}{r^4} \sqrt{10} \quad (3)$$

The magnetic moment m (A m^2) is typically expressed as $m = M\rho V$, where M ($\text{A m}^2/\text{kg}$) is the specific magnetization, ρ is the density, and $V = (4/3)\pi R^3$ is the volume of the particle. Thus, at the surface of the particle

$$\langle |\Delta \mathbf{B}|^2 \rangle^{1/2} \approx \frac{\sqrt{10}}{3} \frac{\mu_0 M \rho l}{R} \quad (4)$$

The key feature of eq 4 is that the magnetic field gradient at the surface of a uniformly magnetized sphere scales inversely with the radius of the sphere. While macroscopic particles cannot induce molecular-scale field gradients, nanoscopic particles can. For instance, a magnetically saturated 10 nm diameter sphere of Fe_3O_4 generates a field gradient of 600 G/nm at its surface (see Table 1 for material parameters). Such a field gradient overwhelms the ~ 60 G difference in Py/DMA due to hyperfine coupling and is far stronger than any field gradient that can be generated with macroscopic coils.

There are two options for how to express the specific magnetization, M . For particles large enough to be ferromagnetic (but still small enough to be a single domain), $M = M_s$, where M_s is the saturation magnetization. In this case the particle has a maximal effect on the rate of ISC, but this enhancement is largely independent of the external magnetic field.

For particles smaller than the superparamagnetic transition, magnetization occurs only in the presence of an external field. A uniaxial superparamagnetic crystal aligned with an applied field H has specific magnetization

$$M = M_s \tanh \left[\frac{M_s \rho V H}{k_B T} \right] \quad (5)$$

where $k_B T$ is the thermal energy. Combining eqs 1, 4, and 5 yields a nanoparticle-enhanced time scale for ISC:

$$\tau_{\text{np}}^{-1} = \frac{\sqrt{10} g \mu_0 \mu_B M_s \rho l}{3\pi \hbar R} \tanh \left[\frac{M_s \rho V H}{k_B T} \right] \quad (6)$$

where the expression has been calculated for radical pairs randomly distributed and randomly oriented on the surface of a nanoparticle, but with the nanoparticle axis parallel to \mathbf{H} . While eq 6 implies no ISC in the absence of an applied field, in reality superparamagnetic fluctuations lead to ISC even when $H = 0$. The effect of such fluctuations is discussed below.

Figure 3 plots the time scale of nanoparticle-enhanced ISC for radical pairs separated by $l = 1$ nm and randomly oriented and distributed on the surface of an Fe_3O_4 nanoparticle. At small particle radius R , the increase in magnetic susceptibility for an increase in R outweighs the decrease in field gradient. At large R the particle becomes magnetically saturated, so $M = M_s$ and $\tau_{\text{np}} \propto R$. The significant feature of Figure 3 is that nanoparticle-enhanced ISC occurs more than an order of magnitude faster than the hyperfine rate in the absence of a nanoparticle.

Equation 6 is valid only in the limit where the magnetic relaxation of the nanoparticle is fast compared to ISC, so the radical pair sees only the average field. Otherwise magnetic fluctuations become important. The time scale of superparamagnetic relaxation is $\tau_{\text{SPM}} = \tau_0 e^{K V / k_B T}$, where K is the magnetocrystalline anisotropy and τ_0 is a weakly temperature dependent “attempt frequency” for magnetization reversal. This time is also plotted in Figure 3.

In the opposite limit, $\tau_{\text{SPM}} \gg \tau_{\text{np}}$, the molecule always sees the saturated magnetic field of the nanoparticle (the direction of magnetization is irrelevant if the nanoparticle is uniformly coated with molecules), and the tanh term should be dropped from eq 6. The nanoparticle still enhances the rate of ISC, but the enhancement is independent of an external magnetic field.

TABLE 1: ISC Induced by Magnetic Nanoparticles^a

| material | M_s , (A m ²)/kg | ρ , kg/m ³ | K , J/m ³ | τ_0 , s | R , nm | τ_{SPM} , s | $\tau_{\text{np}}(\text{SPM}, 100 \text{ G})$, s | $\tau_{\text{np}}(\text{FM})$, s |
|--|--------------------------------|----------------------------|------------------------|-----------------------|----------|-------------------------|---|-----------------------------------|
| Fe ₃ O ₄ ⁵¹ | 43 | 5210 | 4.7×10^4 | 9×10^{-13} | 2.5 | 1.9×10^{-12} | 4.2×10^{-9} | |
| | | | | | 5 | 3.6×10^{-10} | 1.1×10^{-9} | |
| | | | | | 7.5 | 5.3×10^{-4} | | 4.5×10^{-10} |
| Ni ⁵²⁻⁵⁴ | 58.6 | 8912 | 4.2×10^4 | 10^{-10} | 2.5 | 2.0×10^{-10} | 7.8×10^{-10} | |
| | | | | | 5 | 2.1×10^{-8} | | 1.3×10^{-10} |
| | | | | | 7.5 | 6.9×10^{-3} | | 1.9×10^{-10} |
| Co ⁵⁵⁻⁵⁷ | 151 | 8860 | 5.7×10^4 | 5.5×10^{-11} | 2.5 | 1.3×10^{-10} | | 2.5×10^{-11} |
| | | | | | 5 | 7.8×10^{-8} | | 5.0×10^{-11} |
| | | | | | 7.5 | 2.4 | | 7.5×10^{-11} |

^a Material parameters are as defined in the text. τ_{SPM} = superparamagnetic relaxation time. When $\tau_{\text{SPM}} < \tau_{\text{np}}$, τ_{np} is calculated in the superparamagnetic (SPM) limit (eq 11). When $\tau_{\text{SPM}} > \tau_{\text{np}}$, τ_{np} is calculated in the ferromagnetic (FM) limit (i.e., setting $M = M_s$). A Co nanoparticle with a radius of 2.5 nm can induce ISC in Py/DMA more than 200 times faster than the background rate from hyperfine coupling.

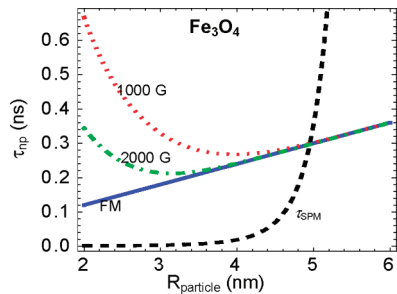


Figure 3. Spin relaxation times for radical pairs near the surface of an Fe₃O₄ nanoparticle. Parameters are the same as in Table 1. Dotted red and dotted–dashed green lines are for superparamagnetic particles in external fields, the solid blue line is for ferromagnetic particles, and the dashed black line shows the superparamagnetic relaxation time.

The material properties of many magnetic nanoparticle samples have been measured, allowing us to estimate the magnitude of the putative nanomagnetic enhancement of ISC. Relevant parameters for some materials are given in Table 1. The estimates in this table show that magnetic nanocrystals of reasonable size and composition can accelerate the rate of ISC in nearby radical pairs by several-hundred-fold.

3. Quantum Theory of ISC near a Magnetic Nanostructure

In the previous section we used intuitive arguments to estimate the time scale of ISC in radical pairs near magnetic nanostructures. Here we perform a more detailed calculation that includes the hyperfine and nanomagnetic interactions on an equal footing. The development parallels that of refs 33 and 49 with the addition of the magnetic field from the nanostructure.

A single spin subject to a static magnetic field \mathbf{B} evolves under the Schrödinger equation

$$i\hbar \frac{\partial \psi}{\partial t} = H\psi \quad (7)$$

with $H = -g\mu_B \mathbf{B} \cdot \mathbf{S}/\hbar$, where $\mathbf{S} = (\hbar/2)\boldsymbol{\sigma}$ is the electron spin operator ($\boldsymbol{\sigma}$ is the vector of Pauli matrices) and the local field \mathbf{B} incorporates both external and hyperfine contributions. We assume that the g -factor is isotropic. The solution to eq 7 is well-known to be $\psi(t) = U(t)\psi_0$, with

$$U(t) = \begin{pmatrix} \cos(\omega t/2) + ib_z \sin(\omega t/2) & (ib_x + b_y) \sin(\omega t/2) \\ (ib_x - b_y) \sin(\omega t/2) & \cos(\omega t/2) - ib_z \sin(\omega t/2) \end{pmatrix} \quad (8)$$

where $\omega = g\mu_B B/\hbar$ and $b_i = \mathbf{B} \cdot \hat{\mathbf{i}}/B$. This solution corresponds to circular motion on the Bloch sphere at frequency ω and about the direction of \mathbf{B} .

For a pair of spins, we take the Hamiltonian $H = -g\mu_B(\mathbf{B}_1 \cdot \mathbf{S}_1 + \mathbf{B}_2 \cdot \mathbf{S}_2)/\hbar$. By omitting contributions containing $\mathbf{S}_1 \cdot \mathbf{S}_2$, we imply that exchange and dipolar interactions are weak, i.e., that the electrons are separated by >1 nm. Nothing in the Hamiltonian couples the motion of the spins, so the time-evolution operator for the two-spin system is simply the direct product of the one-spin operators:

$$U_{\text{Tot}} = U_1 \otimes U_2$$

We take as our initial condition a pure singlet:

$$|\psi_0\rangle = \frac{1}{\sqrt{2}}(|\uparrow\downarrow\rangle - |\downarrow\uparrow\rangle)$$

and define an initial density matrix $\rho_0 = |\psi_0\rangle\langle\psi_0|$. The density matrix at time t is

$$\rho(t) = U_{\text{Tot}}\rho_0 U_{\text{Tot}}^\dagger$$

We introduce singlet and triplet projection operators

$$Q_S = \frac{1}{4} - \frac{1}{4}\boldsymbol{\sigma}_1 \cdot \boldsymbol{\sigma}_2$$

$$Q_T = \frac{3}{4} + \frac{1}{4}\boldsymbol{\sigma}_1 \cdot \boldsymbol{\sigma}_2$$

and calculate the probability of being in a singlet state at time t using the usual prescription $P_S(t) = \text{Tr}[Q_S \rho(t)]$. Doing so leads to a singlet probability:

$$P_S(t) = \left[\cos(\omega_1 t/2) \cos(\omega_2 t/2) + \frac{\mathbf{B}_1 \cdot \mathbf{B}_2}{|B_1||B_2|} \sin(\omega_1 t/2) \sin(\omega_2 t/2) \right]^2 \quad (9)$$

where $\omega_i = g\mu_B B_i/\hbar$. Equation 9 shows that if $\mathbf{B}_1 = \mathbf{B}_2$, then $P_S(t) = 1$ for all times; i.e., a uniform field does not induce ISC. When the spins are in a heterogeneous environment, we are interested in the ensemble-average of eq 9:

$$\langle P_S(t) \rangle = \int P_S(t) P(\mathbf{B}_1, \mathbf{B}_2) d\mathbf{B}_1 d\mathbf{B}_2 \quad (10)$$

where $P(\mathbf{B}_1, \mathbf{B}_2)$ is the joint probability density of \mathbf{B}_1 and \mathbf{B}_2 .

Schulten and Wolynes evaluated this average for the special case where \mathbf{B}_1 and \mathbf{B}_2 are selected from independent 3-dimensional Gaussian distributions, and also the case of independent Gaussian fields plus a uniform external field. The distribution of effective magnetic fields due to hyperfine interactions is calculated from the hyperfine coupling of electron i with neighboring nuclear spin k :

$$H_{\text{hf}} = \sum_k a_{ik} \mathbf{S}_i \cdot \mathbf{I}_k \quad (11)$$

where \mathbf{S} is the electron spin operator, \mathbf{I} is the nuclear spin operator, and a_{ik} is the isotropic nuclear hyperfine coupling constant. When each electron is coupled to many randomly oriented nuclei, the cumulative effect is equivalent to a quasi-static magnetic field, selected from a 3-dimensional Gaussian distribution:

$$P(\mathbf{B}_i) d\mathbf{B}_i = \frac{1}{(2\pi\sigma_i^2)^{3/2}} \exp\left[-\frac{|\mathbf{B}_i|^2}{2\sigma_i^2}\right] d\mathbf{B}_i \quad (12)$$

with variance

$$\sigma_i^2 = \frac{1}{3} \sum_k a_{ik}^2 I_k(I_k + 1) \quad (13)$$

where I_k is the nuclear spin quantum number (1/2 for ^1H and ^{13}C , 1 for ^{14}N).

The hyperfine fields at the locations of the two electrons are statistically independent, so $\Delta B_{\text{rms}} = [3(\sigma_1^2 + \sigma_2^2)]^{1/2}$. Using the semiclassical approximation of eq 1

$$\tau_{\text{HFC}}^{-1} \approx \frac{g\mu_B}{\pi\hbar} \sqrt{3(\sigma_1^2 + \sigma_2^2)} \quad (14)$$

For the model acceptor/donor system pyrene/dimethylaniline (Py/DMA), the hyperfine coupling constants provided by Schulten and Wolynes⁴⁹ yield $\sigma_{\text{Py}} = 5.7$ G and $\sigma_{\text{DMA}} = 18.5$ G,

implying $\tau_{\text{HFC}} \approx 5$ ns. This rough estimate is in good agreement with more detailed calculations.

In the absence of a dc bias field, the hyperfine mechanism populates all three triplet states, with quasi-steady-state populations in the ratio $S_0:T_+:T_0:T_- = 1/3:2/9:2/9:2/9$, assuming an initial S_0 state (see the Appendix for a derivation). When the external field exceeds the strength of the hyperfine fields, the T_+ and T_- states become energetically inaccessible, so the quasi-steady-state populations become $S_0:T_0 = 1/2:1/2$.

In the general case where \mathbf{B}_1 and \mathbf{B}_2 are neither independent nor Gaussian, the integral in eq 10 is not analytically tractable. We resorted to *Monte Carlo* simulations to calculate the spin evolution in several physically realistic scenarios. Simulations were first validated against the analytical results of Kubo for a single spin^{36,37} and Schulten and Wolynes for spin pairs³⁸ in Gaussian random fields. These formulas are given in the Appendix. Figure 4 shows that in both cases the numerical results agree quantitatively with the analytical formulas.

Figure 4 illustrates the interesting feature that neither the single-spin nor the two-spin states ever become isotropically distributed on the Bloch sphere. This feature is a consequence of static disorder: each spin precesses about a random axis on the Bloch sphere, but all such orbits pass through the initial spin orientation. Thus, the system maintains some memory of its initial condition. Dynamic disorder washes out this memory effect, causing all spins to randomize at long times.

3.1. Application to Ferromagnetic Nanocrystals. We treat a ferromagnetic nanocrystal as a uniformly magnetized sphere of radius R . Radical spin pairs are assigned to points $(\mathbf{r}_1, \mathbf{r}_2) = (\mathbf{r} + l/2, \mathbf{r} - l/2)$, where $r \geq R + l/2$. The vectors \mathbf{r} and \mathbf{l} are of fixed length, but random orientation. For each radical the local magnetic field is the sum of the dipole field (eq 2) and a Gaussian-distributed hyperfine field with standard deviation given by eq 13. The hyperfine fields lead to ISC at a background rate even in the absence of a magnetic nanostructure. The singlet probability as a function of time (eq 9) is averaged over all radical pairs (eq 10). We take as a model system the Py/DMA couple with $l = 1$ nm, and use material properties appropriate to Fe_3O_4 (Table 1).

Figure 5 shows the effect of the magnetic field gradient on ISC. In the absence of any external magnetic field, the spins relax due to the hyperfine fields, reaching a quasi-steady-state singlet probability of 1/3 in a time of about 5 ns (consistent with the rough estimate based on eq 14 and exactly matching the result of Schulten and Wolynes³⁸). When we include the magnetic field of a 20 nm diameter ferromagnetic Fe_3O_4

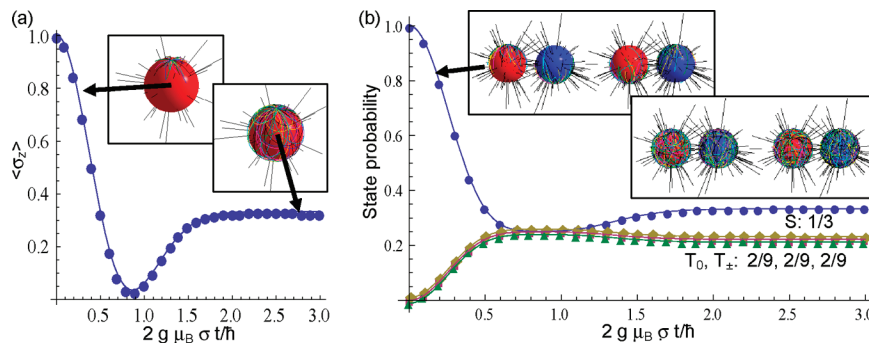


Figure 4. Spin evolution in Gaussian-distributed static magnetic fields. (a) Precession of an ensemble of single spins on the Bloch sphere. Each spin starts at the north pole and follows a circular trajectory around its respective magnetic field (black lines). The ensemble-averaged z -projection gives the Kubo–Toyabe relaxation function. (b) Intersystem crossing in an ensemble of spins initially in a singlet state. The three triplet probabilities have been offset slightly for clarity; each asymptotically reaches 2/9. Red and blue spheres represent the Bloch spheres of the two radicals, and black lines represent Gaussian-distributed magnetic fields. In both panels, points are from a Monte Carlo simulation of 10^4 spins, lines are analytical results, and all magnetic fields are chosen from independent 3-dimensional Gaussian distributions with standard deviation σ .

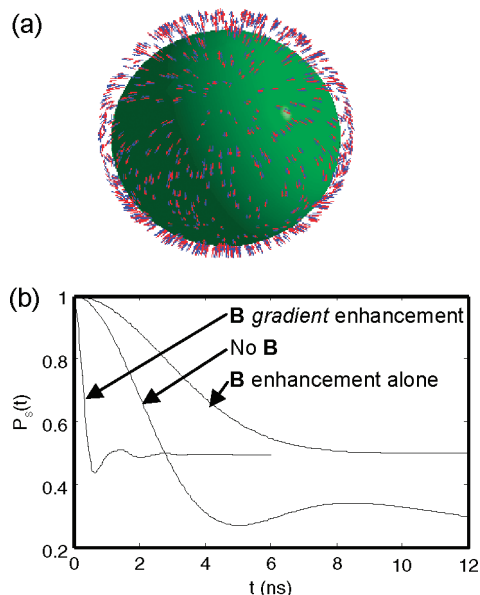


Figure 5. Intersystem crossing near a 20 nm diameter ferromagnetic nanocrystal. (a) Radical pairs distributed on the surface of the nanocrystal. Red and blue arrows represent the nanoparticle field at the location of Py and DMA, respectively. (b) Singlet probability for the Py/DMA radical ion pair, incorporating effects of hyperfine and local magnetic fields.

nanoparticle, but neglect the gradient in this field (i.e., we apply the same field $\mathbf{B}(\mathbf{r})$ to spins at $\mathbf{r} \pm 1/2$), the conventional magnetic field effect is observed: the quasi-steady-state singlet probability is increased to $1/2$, and ISC occurs more slowly than in the absence of a magnetic field. However, if we include the magnetic gradient and calculate the dipolar field separately for each spin, then the rate of ISC is dramatically accelerated: the quasi-steady-state singlet probability of $1/2$ is reached in 0.6 ns.

We investigated the effect of geometry by varying the diameter of the nanoparticle and the distance of the radical pair from the nanoparticle surface. Figure 6 shows these results. Increasing either of these distances decreases the magnitude of gradient-enhanced ISC. However, substantial enhancement in the rate of ISC is still observed for particles as large as 30 nm in diameter.

3.2. Application to Superparamagnetic Nanocrystals. In the case of superparamagnets, the magnetization depends on the applied field. We considered a 5 nm diameter Co nanoparticle with parameters from Table 1. The magnetization was calculated according to eq 5, and radical pairs were placed around the particle as above. Again we included the effect of hyperfine coupling by introducing Gaussian-distributed random fields at the location of each spin. We compared the time evolution of the singlet probability for Py/DMA pairs in homogeneous solution to pairs within 1 nm of the surface of the particle as a function of the applied magnetic field. Figure 7 shows that the applied field has a dramatically different effect on radical pairs near the nanoparticle, compared to pairs in homogeneous solution. As the field increases, pairs near the nanoparticle undergo ISC more rapidly, while pairs in homogeneous solution undergo ISC more slowly. In both cases the long-time singlet probability shifts from $P_S(\infty) = 1/3$ to $P_S(\infty) = 1/2$ as the field increases.

3.3. Effects on Reaction Outcomes. What is the effect of enhanced ISC on the final outcome of a reaction? The answer depends on the relative rates of ISC and the singlet and triplet

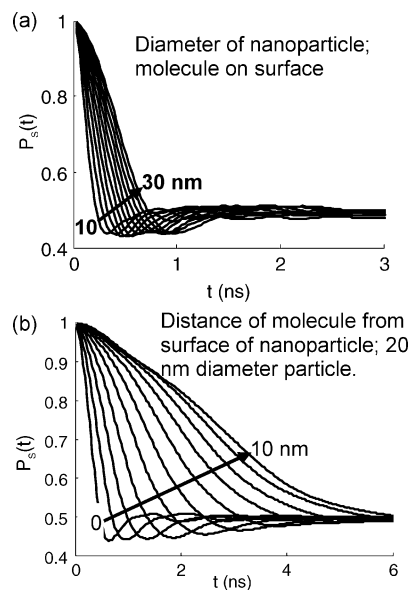


Figure 6. ISC in different geometries: (a) effect of the radius of a ferromagnetic nanoparticle, (b) effect of the distance from the surface of the nanoparticle for a 20 nm diameter particle. ISC curves were calculated for Py/DMA near Fe_3O_4 , using the same parameters as in Figure 5. Each curve was calculated from a Monte Carlo simulation of 10^5 spin pairs.

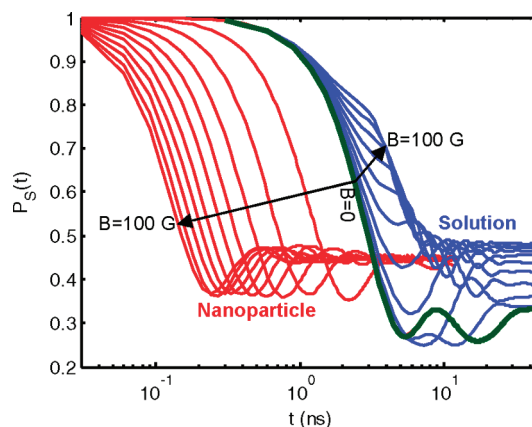
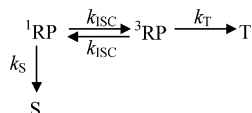


Figure 7. A magnetic field increases the speed of ISC near a 5 nm diameter superparamagnetic Co nanocrystal (red), but slows ISC in homogeneous solution (blue). Green shows the zero-field evolution, dominated by hyperfine coupling.

reactions. If singlet and triplet reactions are both slow relative to ISC, then only the quasi-steady-state singlet probabilities are relevant. In this case, the nanocrystal and a uniform magnetic field have the same effect of *increasing* the steady-state singlet population (from $1/3$ to $1/2$) and *decreasing* the extent of ISC.

If singlet and triplet reactions occur on the same time scale as ISC, then the rate of ISC is important. ISC occurs through quantum interference effects, and thus does not follow simple exponential kinetics. Nonetheless, one may choose to ignore the wiggles in, e.g., Figures 5–7, and to describe the dynamics with a characteristic rate, k_{ISC} . Under most cases of nanomagnetic enhancement, the uniform background field is strong enough to lead to quasi-steady-state singlet populations of 0.5 (see, e.g., Figures 5–7), implying $k_{\text{ISC}} \approx 1/2t_e$, where t_e is the time for $\langle P_S(t) \rangle$ to relax 63% of the way to its quasi-steady-state value. Under these admittedly crude approximations, a generic reaction scheme is



where we assume all reactants are in the state ${}^1\text{RP}$ at $t = 0$. Solving the kinetic equations for this scheme yields a long-time branching ratio:

$$\frac{[\text{S}]}{[\text{T}]} = \frac{k_{\text{S}}}{k_{\text{ISC}}} + \frac{k_{\text{S}}}{k_{\text{T}}} \quad (15)$$

Equation 15 provides a means to estimate the effect of a change in k_{ISC} on the final outcome of a photochemical reaction.

3.4. Effects of Dynamic Fields. Thus far we have only considered static magnetic fields. The local magnetic fields may fluctuate because of (1) time-varying external fields, (2) thermal fluctuations in a superparamagnetic nanoparticle, (3) motion of the spin-bearing molecules, and (4) hopping of radical electrons between molecules. Here we discuss the effects of mechanisms 2 and 3, both of which may be hard to control experimentally. Mechanism 4 is most relevant in solid-state systems or highly concentrated solutions.

In the absence of an external field, the magnetization of a superparamagnetic nanoparticle fluctuates, with typical magnitude M_{s} and typical correlation time τ_{SPM} . These fluctuating random fields are sufficient to induce ISC. We now estimate the time scale of this fluctuation-induced ISC. During an interval τ_{SPM} , the two electrons in a radical pair accumulate a relative phase difference:

$$\Delta\theta_1 \approx \frac{g\mu_{\text{B}}\Delta B}{\hbar} \tau_{\text{SPM}}$$

After time τ_{SPM} the magnetic field chooses another orientation at random. After N steps, the total accumulated phase difference is approximately $\Delta\theta_N \approx \Delta\theta_1(N/2)^{1/2}$. The factor of $1/\sqrt{2}$ arises because $\Delta\theta$ is undergoing a 2-dimensional random walk on the Bloch sphere, and the directions of successive steps are uncorrelated. As in section 2, we estimate that ISC occurs when the accumulated phase difference $\Delta\theta_N \approx \pi$. We make the substitution $N = \tau_{\text{ISC}}/\tau_{\text{SPM}}$ and use eq 4 for ΔB , dropping the factor of $(\sqrt{10})/3 \approx 1$. ISC occurs in a time

$$\tau_{\text{ISC}}^{-1} \approx \frac{\tau_{\text{SPM}}}{2} \left(\frac{g\mu_{\text{B}}M_{\text{s}}\rho l}{\pi\hbar R} \right)^2 \quad (16)$$

The same argument applies to incorporate the effect of molecular tumbling on radical pairs near a magnetic nanoparticle with fixed magnetization M . In this case, the correlation time of ΔB is given by the tumbling time τ_{rot} , so

$$\tau_{\text{ISC}}^{-1} \approx \frac{\tau_{\text{rot}}}{2} \left(\frac{g\mu_{\text{B}}M\rho l}{\pi\hbar R} \right)^2 \quad (17)$$

Equations 16 and 17 are only valid in the limit where the individual step size $\Delta\theta_1 \ll \pi$. Both formulas show that, as the magnetic fluctuations become fast, ISC slows. This behavior is a hallmark of motional narrowing. We note that the time scales of ISC calculated without the inclusion of molecular tumbling (<1 ns) are shorter than or comparable to the tumbling time for

small molecules in solutions of moderate viscosity. Thus, we do not expect motional narrowing due to molecular tumbling to decrease significantly the magnitude of nanomagnetic catalysis of ISC, even for small molecules in low-viscosity solutions.

One could investigate further the detailed form of $\langle P_{\text{S}}(t) \rangle$ for various models of the evolution of the random magnetic field (e.g., a Gaussian–Markovian process, an n -state discrete jump model), as has been done for single spins in application to muon relaxation.⁵⁰ However, given the complexity of real experiments, such an effort does not seem justified until the basic phenomena predicted here have been observed. A more detailed treatment should include inter- and intramolecular motion of the spins, fluctuations of the magnetic nanostructure, anisotropy in the g -factors and the hyperfine coupling constants, and dipolar, exchange, and possibly spin–orbit interactions. Such effects may lead to corrections to the model presented here, but are not expected to change the basic phenomena.

4. Discussion

We have proposed a novel form of heterogeneous catalysis in which the catalytic effect is mediated by short-range magnetic interactions. Unlike traditional heterogeneous catalysis, this effect does not require molecular contact. Realistic magnetic nanostructures generate magnetic field gradients that are strong enough to dominate the rate of intersystem crossing in nearby radical pairs. While the discussion has focused on spherical magnetic nanoparticles, similar arguments could be applied to the field distribution near ferromagnetic domain boundaries or other materials with heterogeneous magnetic surface texture. Indeed, one can imagine using gradient-induced ISC as a probe of magnetic surface texture, with a spatial resolution determined by the size of the molecules undergoing ISC.

Spin statistics play an important role in electron–hole recombination in organic conductors, in photophysical properties of molecules, and in reaction chemistry. Hybrid organic/magnetic nanostructures may open new avenues for control in each of these domains. Radical reactions are widespread in biology and chemistry, and every radical reaction begins with the separation of two paired electrons. Magnetic nanostructures have the potential to exert a large effect on the efficiency of this initial separation process. Experiments to test these predictions are under way.

Acknowledgment. I thank Nan Yang and Eran Mukamel for helpful discussions. This work was supported in part by the Materials Research Science and Engineering Center of the National Science Foundation under NSF Award Number DMR-02-13805, a Dreyfus New Faculty Award, a DARPA Young Faculty Award, and the Office of Naval Research Young Investigator Program.

Appendix

Here we derive the expressions for the decay of the z -magnetization and the singlet probability for one- and two-spin systems, respectively. Each spin is coupled to a static magnetic field selected from an isotropic 3-dimensional Gaussian distribution.

One-Spin System. A single spin subject to a magnetic field \mathbf{B} evolves as $\psi(t) = U(t)\psi_0$, with $U(t)$ given by eq 8. The z -component of the magnetization is $M_z(t) = \langle \psi(t) | S_z | \psi(t) \rangle$. If a particle starts in the spin up, or

$$\begin{pmatrix} 1 \\ 0 \end{pmatrix}$$

state, the z -magnetization is

$$M_z(t) = \frac{\hbar}{2} [\cos^2(\omega t/2) - (b_x^2 + b_y^2 - b_z^2) \sin^2(\omega t/2)]$$

In the presence of hyperfine couplings to many atomic nuclei, the effective magnetic field follows a 3-dimensional Gaussian distribution, with probability density

$$P(B) dB = \frac{4\pi B^2}{(2\pi\sigma^2)^{3/2}} \exp\left[-\frac{B^2}{2\sigma^2}\right] dB \quad (\text{A1})$$

where σ is a measure of the width of the Gaussian, and $\langle B^2 \rangle = 3\sigma^2$.

The ensemble-average z -magnetization is $\langle M_z(t) \rangle = \int_0^\infty M_z(t) P(B) dB$, which evaluates to the Kubo–Toyabe formula

$$\langle M_z(t) \rangle / \langle M_z(0) \rangle = \frac{1}{3} + \frac{2}{3}(1 - \lambda^2 t^2) \exp\left[-\frac{1}{2}\lambda^2 t^2\right]$$

with $\lambda = g\mu_B\sigma/\hbar$. Figure 4a in the main text shows a plot of this function. For comparison to ISC below, we define

$$X \equiv (1 - \lambda^2 t^2) \exp\left[-\frac{1}{2}\lambda^2 t^2\right] \quad (\text{A2})$$

Hence

$$\langle M_z(t) \rangle / \langle M_z(0) \rangle = \frac{1}{3}(1 + 2X)$$

Two-Spin System, Initial Singlet. In the text we showed that the probability of remaining in the singlet state is

$$P_S(t) = \left[\cos(\omega_1 t/2) \cos(\omega_2 t/2) + \frac{\mathbf{B}_1 \cdot \mathbf{B}_2}{|\mathbf{B}_1||\mathbf{B}_2|} \sin(\omega_1 t/2) \sin(\omega_2 t/2) \right]^2$$

We take eq A1 for both $P(B_1)$ and $P(B_2)$. One could choose different values of σ for the two spins, but for simplicity here we assume both values of σ are the same. In this case the joint probability factorizes, so $P(\mathbf{B}_1, \mathbf{B}_2) = P(\mathbf{B}_1) P(\mathbf{B}_2)$. Taking advantage of the fact that $\langle \mathbf{B}_1 \cdot \mathbf{B}_2 \rangle = 0$, we find

$$\langle P_S(t) \rangle = \frac{1}{3}(1 + X + X^2) \quad (\text{A3})$$

where X is as defined in eq A2. Equation A3 is plotted in Figure 4b. At times $t \gg \lambda$, $X \rightarrow 0$, so $\langle P_S \rangle \rightarrow 1/3$.

Each of the three triplet states is occupied with equal time-dependent probability, given by

$$\langle P_T(t) \rangle = \frac{1}{9}(2 - X - X^2)$$

The long-time occupation probabilities are in the ratios $S_0:T_+:T_0:T_- = 1/3:2/9:2/9:2/9$. These ratios differ from the equilibrium ratios of $1/4:1/4:1/4:1/4$ because static random fields cannot create a homogeneous distribution of spins on the Bloch sphere. Only dynamic heterogeneity can lead to thermal equilibrium. At long times the nuclear spins reorient themselves, and the occupancy of each spin state approaches the statistical average value of $1/4$.

Two-Spin System, Initial Triplet. An argument similar to that given above applies to spin evolution in Gaussian random fields starting from a triplet state. Starting in the T_0 state, the time-dependent amplitudes in each of the four spin states are

$$\langle P_{T_0}(t) \rangle = \frac{1}{3}(1 + X + X^2)$$

and

$$\langle P_{T_+}(t) \rangle = \langle P_{T_-}(t) \rangle = \langle P_{S_0}(t) \rangle = \frac{1}{9}(2 - X - X^2)$$

The long-time occupation probabilities are in the ratio $S_0:T_+:T_0:T_- = 2/9:2/9:3/9:2/9$. Thus, the probability of remaining in one of the three triplet states is $7/9$.

Starting in the T_+ state, the time-dependent amplitudes are

$$\langle P_{T_0}(t) \rangle = \langle P_{S_0}(t) \rangle = \frac{1}{9}(2 - X - X^2)$$

$$\langle P_{T_+}(t) \rangle = \frac{1}{9}(2 + X)^2$$

$$\langle P_{T_-}(t) \rangle = \frac{1}{9}(X - 1)^2$$

The long-time occupation probabilities are in the ratio $S_0:T_+:T_0:T_- = 2/9:4/9:2/9:1/9$. As with an initial T_0 state, the probability of remaining in one of the three triplet states is $7/9$. The results starting in a T_- state are the same, with the substitution $T_+ \leftrightarrow T_-$.

References and Notes

- (1) Steiner, U. E.; Ulrich, T. *Chem. Rev.* **1989**, *89*, 51.
- (2) Turro, N. J. *Modern Molecular Photochemistry*; University Science Books: Herndon, VA, 1991.
- (3) Nagakura, S.; Hayashi, H.; Azumi, T. *Dynamic Spin Chemistry: Magnetic Controls and Spin Dynamics of Chemical Reactions*; Wiley-Kodansha: Tokyo, 1998.
- (4) Boehme, C.; Lips, K. *Phys. Rev. B* **2003**, *68*, 245105.
- (5) McCamey, D. R.; Seipel, H. A.; Paik, S. Y.; Walter, M. J.; Borys, N. J.; Lupton, J. M.; Boehme, C. *Nat. Mater.* **2008**, *7*, 723.
- (6) Lupton, J. M.; Boehme, C. *Nat. Mater.* **2008**, *7*, 598.
- (7) Groff, R. P.; Suna, A.; Avakian, P.; Merrifield, R. E. *Phys. Rev. B* **1974**, *9*, 2655.
- (8) Atkins, P. W.; Evans, G. T. *Mol. Phys.* **1975**, *29*, 921.
- (9) Weiss, E. A.; Ratner, M. A.; Wasielewski, M. R. *J. Phys. Chem. A* **2003**, *107*, 3639.
- (10) Chidsey, C. E. D.; Takiff, L.; Goldstein, R. A.; Boxer, S. G. *Proc. Natl. Acad. Sci. U.S.A.* **1985**, *82*, 6850.
- (11) Sakaguchi, Y.; Hayashi, H. *J. Phys. Chem.* **1984**, *88*, 1437.
- (12) Weller, A.; Staerk, H.; Treichel, R. *Faraday Discuss. Chem. Soc.* **1974**, *78*, 271.
- (13) Fujiwara, Y.; Aoki, T.; Haino, T.; Fukazawa, Y.; Tanimoto, Y.; Nakagaki, R.; Takahira, O.; Okazaki, M. *J. Phys. Chem. A* **1997**, *101*, 6842.
- (14) Scaiano, J. C.; Abuin, E. B.; Stewart, L. C. *J. Am. Chem. Soc.* **1982**, *104*, 5673.
- (15) Rintoul, I.; Wandrey, C. *J. Polym. Sci., Part A: Polym. Chem.* **2009**, *47*, 373.

- (16) Ushakova, M. A.; Chernyshev, A. V.; Taraban, M. B.; Petrov, A. K. *Eur. Polym. J.* **2003**, *39*, 2301.
- (17) Doubleday Jr, C.; Turro, N. J.; Wang, J. F. *Acc. Chem. Res.* **1989**, *22*, 199.
- (18) Cozens, F. L.; Scaiano, J. C. *J. Am. Chem. Soc.* **1993**, *115*, 5204.
- (19) Turro, N. J.; Kraeutler, B. *J. Am. Chem. Soc.* **1978**, *100*, 7432.
- (20) Turro, N. J. *Proc. Natl. Acad. Sci. U.S.A.* **1983**, *80*, 609.
- (21) Ritz, T.; Adem, S.; Schulten, K. *Biophys. J.* **2000**, *78*, 707.
- (22) Mouritsen, H.; Ritz, T. *Curr. Opin. Neurobiol.* **2005**, *15*, 406.
- (23) Rodgers, C. T.; Hore, P. J. *Proc. Natl. Acad. Sci. U.S.A.* **2009**, *106*, 353.
- (24) Gegeer, R. J.; Casselman, A.; Waddell, S.; Reppert, S. M. *Nature* **2008**, *454*, 1014.
- (25) Petta, J. R.; Johnson, A. C.; Taylor, J. M.; Laird, E. A.; Yacoby, A.; Lukin, M. D.; Marcus, C. M.; Hanson, M. P.; Gossard, A. C. *Science* **2005**, *309*, 2180.
- (26) Maze, J. R.; Stanwix, P. L.; Hodges, J. S.; Hong, S.; Taylor, J. M.; Cappellaro, P.; Jiang, L.; Dutt, M. V. G.; Togan, E.; Zibrov, A. S.; Yacoby, A.; Walsworth, R. L.; Lukin, M. D. *Nature* **2008**, *455*, 644.
- (27) Sun, C. J.; Wu, Y.; Xu, Z.; Hu, B.; Bai, J.; Wang, J. P.; Shen, J. *Appl. Phys. Lett.* **2007**, *90*, 232110.
- (28) Hu, B.; Wu, Y.; Zhang, Z.; Dai, S.; Shen, J. *Appl. Phys. Lett.* **2006**, *88*, 022114.
- (29) Kumar, P.; Kumar, H.; Chand, S.; Jain, S. C.; Kumar, V.; Kumar, V.; Pant, R. P.; Tandon, R. P. *J. Phys. D* **2008**, *41*, 185104.
- (30) Scaiano, J. C.; Monahan, S.; Renaud, J. *Photochem. Photobiol.* **1997**, *65*, 759.
- (31) Herve, P.; Nome, F.; Fendler, J. H. *J. Am. Chem. Soc.* **1984**, *106*, 8291.
- (32) Wigner, E. Z. *Phys. Chem. B* **1933**, *23*, 28–32.
- (33) Petzinger, K. G.; Scalapino, D. J. *Phys. Rev. B* **1973**, *8*, 266.
- (34) Atkins, P.; Clugston, M. *Mol. Phys.* **1974**, *27*, 1619.
- (35) Buchachenko, A. L.; Berdinsky, V. L. *Chem. Rev.* **2002**, *102*, 603.
- (36) Kubo, R.; Toyabe, T. In *Magnetic Resonance and Relaxation*; Blinc, R., Ed.; North-Holland: Amsterdam, 1967; p 810.
- (37) Hayano, R. S.; Uemura, Y. J.; Imazato, J.; Nishida, N.; Yamazaki, T.; Kubo, R. *Phys. Rev. B* **1979**, *20*, 850.
- (38) Schulten, K.; Wolynes, P. G. *J. Chem. Phys.* **1978**, *68*, 3292.
- (39) Knapp, E. W.; Schulten, K. *J. Chem. Phys.* **1979**, *71*, 1878.
- (40) Binhi, V. *Int. J. Radiat. Biol.* **2008**, *84*, 569.
- (41) Kirschvink, J. L.; Kobayashi-Kirschvink, A.; Woodford, B. J. *Proc. Natl. Acad. Sci. U.S.A.* **1992**, *89*, 7683.
- (42) Walker, M. M.; Diebel, C. E.; Haugh, C. V.; Pankhurst, P. M.; Montgomery, J. C.; Green, C. R. *Nature* **1997**, *390*, 371.
- (43) Kirschvink, J. L.; Walker, M. M.; Diebel, C. E. *Curr. Opin. Neurobiol.* **2001**, *11*, 462.
- (44) Chignell, C. F.; Sik, R. H. *Photochem. Photobiol.* **1998**, *68*, 598.
- (45) Chalkias, N. G.; Kahawong, P.; Giannelis, E. P. *J. Am. Chem. Soc.* **2008**, *130*, 2910.
- (46) Kaptein, R. *J. Am. Chem. Soc.* **1972**, *94*, 6251.
- (47) Kaptein, R.; Den Hollander, J. A. *J. Am. Chem. Soc.* **1972**, *94*, 6269.
- (48) Griffiths, D. J. *Introduction to Electrodynamics*, 3rd ed.; Prentice Hall: Upper Saddle River, NJ, 1999.
- (49) Schulten, K. *Adv. Solid State Phys.* **1982**, *22*, 61.
- (50) Borgs, P.; Kehr, K. W.; Heitjans, P. *Phys. Rev. B* **1995**, *52*, 6668.
- (51) Goya, G. F.; Berquó, T. S.; Fonseca, F. C.; Morales, M. P. *J. Appl. Phys.* **2003**, *94*, 3520.
- (52) Danan, H.; Herr, A.; Meyer, A. J. P. *J. Appl. Phys.* **1968**, *39*, 669.
- (53) Hou, Y.; Gao, S. *J. Mater. Chem.* **2003**, *13*, 1510.
- (54) Gittleman, J. I.; Abeles, B.; Bozowski, S. *Phys. Rev. B* **1974**, *9*, 3891.
- (55) Aus, M. J.; Cheung, C.; Szpunar, B.; Erb, U.; Szpunar, J. *J. Mater. Sci. Lett.* **1998**, *17*, 1949.
- (56) Eastham, D. A.; Denby, P. M.; Harrison, A.; Kirkman, I. W.; Whittaker, A. G. *J. Phys.: Condens. Matter* **2002**, *14*, 605.
- (57) Andrade, L. H.; Laraoui, A.; Vomir, M.; Muller, D.; Stoquert, J.; Estournes, C.; Beaurepaire, E.; Bigot, J. *Phys. Rev. Lett.* **2006**, *97*, 127401.

JP907113P